A study of biaxial fatigue behavior of a synthetic rubber

J.L.Poisson, F.Lacroix, S.Meo, G.Berton and N.Ranganathan

CERMEL, Laboratoire de Mécanique et Rhéologie, Université François Rabelais de Tours, 7 Avenue Marcel Dassault 37200 Tours France, Email : lacroix@univ-tours.fr

ABSTRACT. *Understanding phenomenon induced by complex fatigue loadings is an important issue for the conception of industrial components. Rubber materials, thanks to their abilities to withstand high deformations, are more and more used in industry. In an ongoing study, an experimental investigation is being carried out to study the effect of multiaxial loadings on the fatigue life of polychloroprene rubber. This material is used for pulleys. Specimen used is a dumbbell type, axisymetric geometry with a reduced section at mid-height. The experimental results indicate that under uniaxial tensile loading a kink in the conventional Haigh diagrams is observed leading to high lives at high R ratio loading as compared to low R ratios. Fractographic studies indicate the presence of crystallographic tongues under high R ratio loading. To reproduce multiaxial conditions on this specimen, combined axial displacements and torsion rotation fatigue tests are performed, according to three different paths, depending on the phase angle between the two axes. Different multiaxial fatigue criteria are used to analyze experimental results.*

INTRODUCTION

Elastomers are more and more used in industrial applications (tyres, belts, pulleys ...) thanks to their interesting mechanical behavior and their diversity. In service conditions, rubber components are subjected to multiaxial loadings. Many studies have been carried out to understand multiaxial fatigue phenomena in a natural rubber (NR). André and al. [1] have built a Haigh diagram to estimate multiaxial fatigue life of a NR. They noticed an increase of fatigue life in high R-Ratio values, due to crystallization under a tensile stress state. In their investigations, Saintier and al. [2] have identified two regions in the Haigh diagram for the NR: positive and negative R-ratio, with $R = \frac{\sigma_{min}}{\sigma_{max}}$.

In previous works [3, 4], dissipated energy density was used as a fatigue criterion under uniaxial fatigue tests, showing encouraging results with this criterion. The aim of this study is to use the same criterion in multiaxial fatigue results and to compare it with first principal stress and strain energy density. To understand the influence of R-Ratio in fatigue behavior, a Haigh diagram is built, where fatigue results are gathered in a graph, in which the absicca represents the average hydrostatic pressure, and the ordinate represents the amplitude of first principal Cauchy stress. In this paper, experimental

conditions are first explained. To calculate the relevant fatigue criteria, an analytical model that determines the material stress-strain law is needed. A second part is developed to highlight the basis of the calculations of this model. At the end, criteria are calculated in two different ways: a global approach which consists of estimating criteria from direct experimental data and a local approach where criteria are determined at a local point of the specimen for a stabilized cycle. Results are plotted and discussed in the final part of the paper.

EXPERIMENTAL INVESTIGATIONS

As multiaxial solicitations, tension-torsion tests were carried out with an electromechanical biaxial fatigue test device BOSE. Those tests were conducted on dumbell specimens (fig.1) which consists of a rubber part, with a gage length about 30 mm, bounded to metal parts at each extremity, which can be attached to the test machine by two screws.

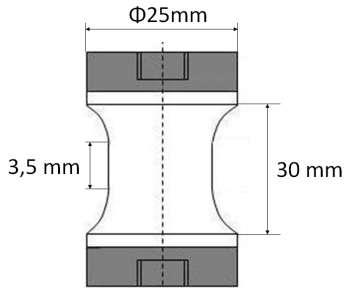

Figure 1. Dumbell specimen

Those specimens were moulded by an injection press device at 175°C, during 4 minutes. The material used in this present work is a vulcanized polychloroprène rubber (CR), filled with N990 carbon black used on pulley applications. Fatigue tests were strain imposed at a single frequency (5Hz) and at room temperature (20° C). Details of biaxial fatigue tests, listed in Figs. 2 and 3 are inspired from [5]. In these figures, U(t) and θ(t) are respectively axial and angular displacements. Three different values of phase angle δ were considered, as shown in Fig. 3.

Investigating on the influence of Rd-ratio[1] in the fatigue life constitutes an important issue, considering that Legorju-jago [6] suggested the crystallization of CR under a tensile stress state. Therefore, three different values of Rd-ratios were chosen for each path. The fatigue test's end life is defined precisely when the specimen is completely broken.

[1] $Rd = \frac{U_{min}}{U_{max}} = \frac{U_m - U_a}{U_m + U_a}$

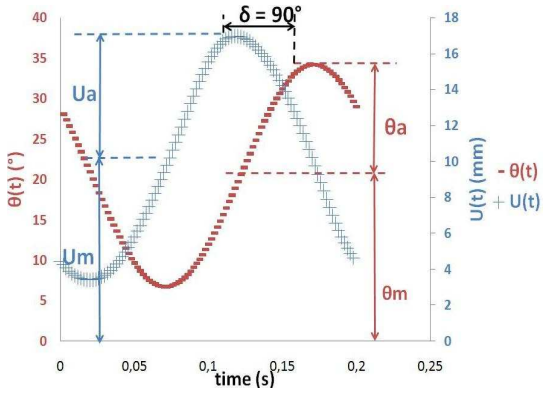

Figure 2. Fatigue cycle in tension-torsion

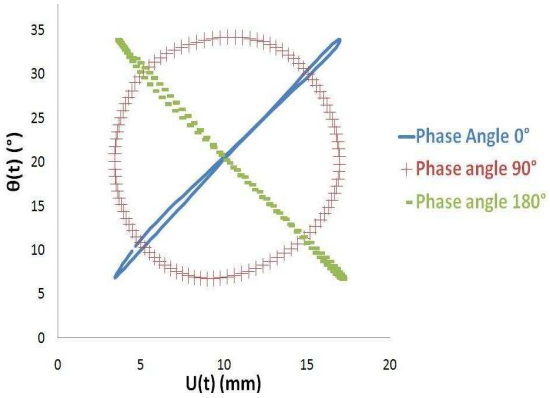

Figure3. Different fatigue paths

To calculate different criteria, such as first principal stress, an analytical model which determines our material's stress-strain laws is needed.

MECHANICAL MODEL

To analyze the fatigue tests results, the knowledge of the stress-strain law is important, considering the material incompressible. Due to their ability to withstand high levels of strains, determining the constitutive model of an elastomer is difficult. Large strain models are also needed. Moreover, to calculate the dissipated energy density criterion, the model must have a dissipative part. Herein, a viscoelastic dissipative part is chosen. Finally, a large deformation Kelvin-Voigt model is used to describe the CR's behavior, where ψ is the hyperelastic strain energy density and φ is the dissipative potential (Fig. 4):

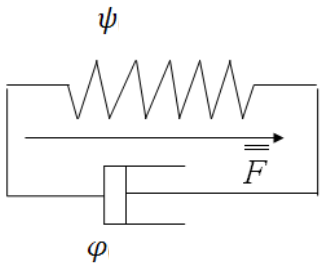

Figure 4. Large deformation Kelvin-Voigt model

To determine this model, it is necessary to introduce the gradient tensor $\overline{\overline{\boldsymbol{F}}} = \frac{\partial \boldsymbol{X}}{\partial \boldsymbol{x}}$, where X is the position of a point in the initial configuration, and x is the position of this point in the actual configuration. In order to simulate tension-torsion kinematics, the gradient tensor is calculated in Eq. 1 from the basis of [7], where L, R are respectively the length

and radius of the cylinder in which we calculate the tensor. Z is the altitude of the point where the tensor is calculated.

$$\overline{\overline{F}} = \begin{pmatrix} \sqrt{\frac{L}{L+u(t)}}\cos(\frac{\theta(t)Z}{L}) & -\sqrt{\frac{L}{L+u(t)}}\sin(\frac{\theta(t)Z}{L}) & -R\frac{\theta(t)}{L}\sqrt{\frac{L}{L+u(t)}}\sin(\frac{\theta(t)Z}{L}) \\ \sqrt{\frac{L}{L+u(t)}}\sin(\frac{\theta(t)Z}{L}) & \sqrt{\frac{L}{L+u(t)}}\cos(\frac{\theta(t)Z}{L}) & R\frac{\theta(t)}{L}\sqrt{\frac{L}{L+u(t)}}\cos(\frac{\theta(t)Z}{L}) \\ 0 & 0 & 1+\frac{u(t)}{L} \end{pmatrix} \quad (1)$$

In this formulation, a Mooney-Rivlin model is used to determine the elastic part (Eq.2) and a dissipative function φ (Eq.3) describe the dissipative part [3], where I_1, I_2 are the first and second invariants of the right Cauchy-Green tensor $\overline{\overline{C}} = \overline{\overline{F}}^T \overline{\overline{F}}$. C_{10}, C_{01} and ν are material parameters. $\overline{\overline{E}} = \frac{1}{2}(\overline{\overline{C}} - \overline{\overline{I}})$ is the Euler-Almansi strain tensor.

$$\rho_0 \psi(I_1, I_2) = C_{10}(I_1 - 3) + C_{01}(I_2 - 3) \quad (2)$$

$$\boldsymbol{\varphi} = \frac{\nu}{2}.\dot{\overline{\overline{E}}} : \dot{\overline{\overline{E}}} \quad (3)$$

From those relationships, the stress-strain law can be given by Eq.4, in the mixed configuration [3], where Π is the first Piola-Kirshoff stress tensor (PK1), ρ_0 the initial material's density and p, a hydrostatic pressure due to the incompressibility condition.

$$\overline{\overline{\Pi}} = 2\rho_0 \overline{\overline{F}} \frac{\partial \psi}{\partial \overline{\overline{C}}} + \overline{\overline{F}} \frac{\partial \boldsymbol{\varphi}}{\partial \dot{\overline{\overline{E}}}} - p\overline{\overline{F}}^{-T} \quad (4)$$

IDENTIFICATION OF PARAMETERS

The Kelvin-Voigt model is composed with three unknown material parameters, which were identified from the most damaging cyclic uniaxial tension fatigue condition. An average between loading and unloading obtained results leads to the hyperelastic part. Then, the dissipative part is calculated with the whole cycle. Optimization's operations were done with a least squares algorithms. Figure 5 shows the final result, showing an acceptable correlation between the experimental and predicted hysteresis loops.

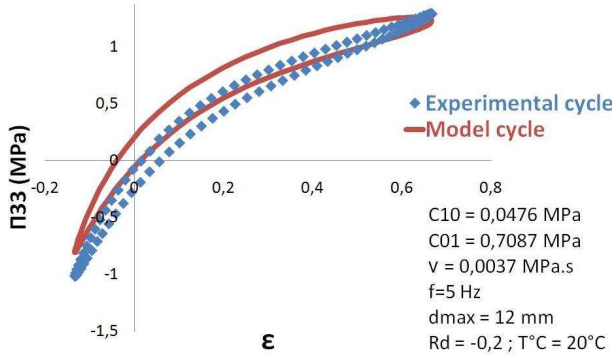

Figure 5. Result of the Kelvin Voigt parameters' identification

FATIGUE CRITERIA

Two ways to analyze fatigue results are developed in this paper: the first one consists on calculating criteria from the raw fatigue data, a global approach. The second is based on the stress-strain law discussed previously, and consists on calculating fatigue criteria at a certain point of the specimen. Unfortunately, some criteria cannot be calculated in both ways.

Maximum principal stress

Many works [2] showed that the first principal stress was responsible of crack opening and propagation in rubber fatigue tests. Accordingly, this parameter is commonly used as a fatigue criterion in rubber's applications.

Strain energy density

Strain energy density is developed from integration of Eq.5 in the loading part of both axial and angular fatigue cycle, where V_h is the gage specimen's volume [8], F the tension load, du an increment of axial displacement, C the torque and $d\theta$ an increment of angular displacement.

$$dW = \frac{1}{V_h}(F.du + C.d\boldsymbol{\theta}) \tag{5}$$

Dissipated energy density

Dissipated energy density is determined in both global approach (by integrating Eq.5 in a whole stabilized fatigue cycle) and local approach. Eq.6 describes the local formulation of dissipated energy density:

$$W_d = \int_{cycle} \overline{\overline{\Pi}} : \dot{\overline{\overline{E}}}.dt \tag{6}$$

RESULTS AND DISCUSSIONS

Figures 6 to 9 shows the fatigue results for the Maximal PK1 maximum principal stress, the strain energy density and the dissipated energy density.

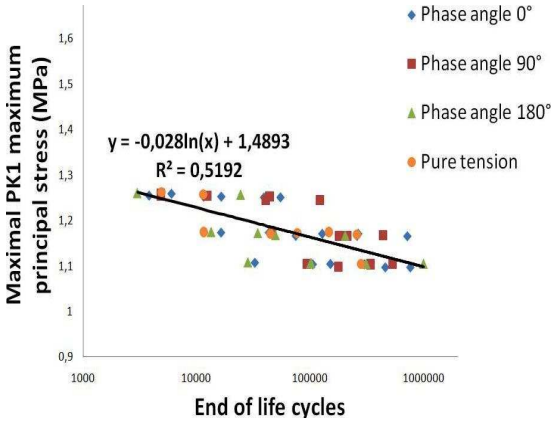

Figure 6. Fatigue results for maximal PK1 maximum principal stress

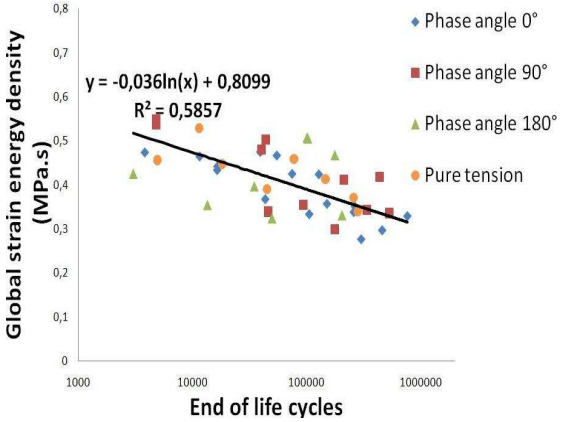

Figure 7. Fatigue results for global strain energy density

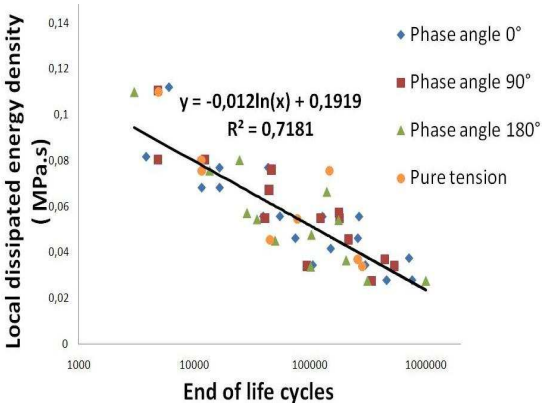

Figure 8. Fatigue results for local dissipated energy density

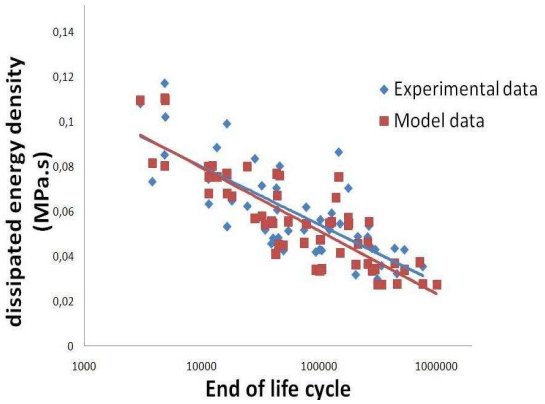

Figure 9. Fatigue results comparison between local and global dissipated energy

Figure 8 shows a good correlation between local dissipated energy density and multiaxial fatigue life for the different paths, with a moderate scatter in results. Moreover, Figure 9 highlights the close results between global and local dissipated energy density. Analysis of these results indicates that dissipated energy seems to be the most relevant critrian as we obtain the best coefficient of correlation irrespective of the loading path.

However, a Haigh diagram is needed to highlight the influence of Rd-ratio on multiaxial fatigue (Fig.10). In this figure, the x-axis represents the average hydrostatic pressure $p = \frac{1}{3}\mathrm{tr}(\bar{\bar{\sigma}})$ and the y-axis the first principal Cauchy stress' amplitude. Fatigue life is

displayed for each condition in multiples of 10^5 cycles. At first sight, this diagram indicates first an influence of phase angle in fatigue behavior, independently from the Rd-ratio. When each path is observed separately, a singularity appears at 0.2 Rd-ratio. It can be observed here that for tests with an Rd raio of 0.2, lives in the range of 122000 to 1000000 cycles are observed, i.e. much higher than those observed at lower Rd valuses. This result itself seems to indicate that at high Rd ratios tha fatigue damage mechanism could be different (probably due to crystallization effects). However, there are not enough results yet to clearly represent tendencies and fatigue life curves.

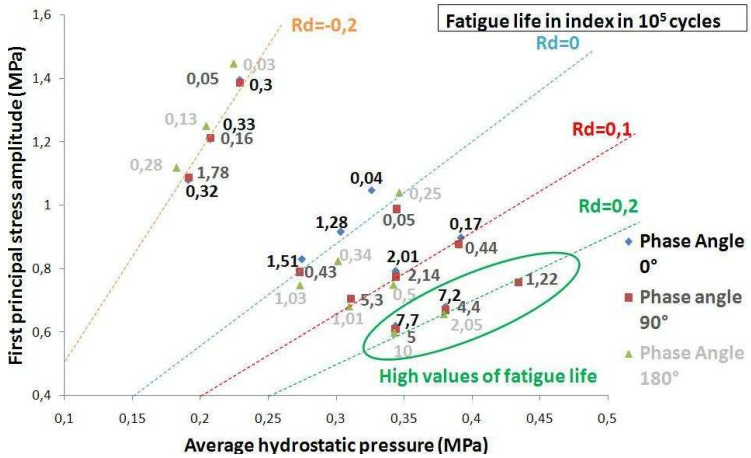

Figure 10. CR's Haigh diagram

FATIGUE FACETS

An observation of morphology in failure surface's specimen is achieved in a SEM (Scanning Electronic Microscope) JEOL 6480 LV, with an aim to find manifestations of crystallization and the understanding fatigue phenomena. In Figure 11a. is displayed a macroscopic view of such a surface.

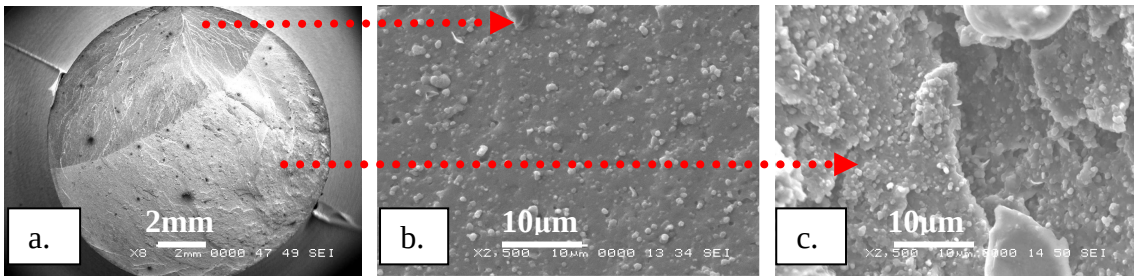

Figure 11. SEM photomicrographs (Secondary Electronic Ionisation)
a. Macroscopic failure surface (x8), b. End of life zone (x2500), c. Fatigue zone (x2500)

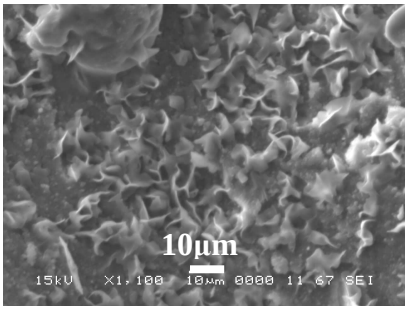

Figure 12. SEM microphotograph of high Rd-ratio uniaxial fatigue failure surface (x1100)

This facet is divided into two regions: a smooth one corresponded to the end of life location (Fig. 11b) and a rough one which seems to be the fatigue failure surface (Fig. 11c). However, expected crystallization's effects are difficult to observe in multiaxial fatigue facets. The photomicrograph in Fig. 12 highlights the presence of tongues, indicative of crystallization phenomenon [6].

CONCLUSION

The present study aimed at understanding multiaxial fatigue behavior of a chloroprene synthetic rubber leads us to a few conclusions:

1) For a given stress ampltude, higher fatigue lives are observed at high Rd ratios irrespective of the loading path
2) Local energy dissipated seems to be the most acceptable fatigue criterion.
3) Local and global dissipated energies are quite comparable showing that the mechanical model developed is very good
4) Fratographic studies (even though not yet complete) indicate the presence of crystallization at high Rd ratios.

REFERENCES

1. André, N., Cailletaud, G., Piques, R. (1999) *Kantschuk Gummi Kunststoffen* **52**, 120-123
2. Saintier, N., Cailletaud, G., Piques, R. (2006) *International Journal of Fatigue* **28**, 530-539
3. Lacroix, F., Meo, S., Berton, G., Chalon, F., Tougui, A., Ranganathan, N. (2005) *Constitutive models for rubber IV*, P.-E. Austrell & L. Kari, London
4. Lu, C. (1991) PhD Thesis, Centre Natinal des Arts et Métiers, France
5. Mars, W.V., Fatemi, A. (2006) *International Journal of Fatigue* **28**, 521-529
6. Legorju-jago, K., Bathias, C. (2002) *International Journal of Fatigue* **24**, 85-92
7. Feng, W.W., Hung, T.K., Chang, G.-L. (1992) *Int. J. Non-Linear Mechanics* **27**, 329-335
8. Mars, W.V., Fatemi, A. (2005) *Fatigue Fract Engng Mater Struct* **28**, 523-538